Bunching-induced optical nonlinearity and instability in cold atoms [Invited]

Joel A. Greenberg,* Bonnie L. Schmittberger, and Daniel J. Gauthier

Department of Physics and the Fitzpatrick Institute for Photonics, Duke University, Durham, NC 27708, USA

*jag27@phy.duke.edu

Abstract: We report a new nonlinear optical process that occurs in a cloud of cold atoms at low-light-levels when the incident optical fields simultaneously polarize, cool, and spatially-organize the atoms. We observe an extremely large effective fifth-order nonlinear susceptibility of $\chi^{(5)} = 7.6 \times 10^{-15}$ (m/V)^4, which results in efficient Bragg scattering via six-wave mixing, slow group velocities ($\sim c/10^5$), and enhanced atomic coherence times ($> 100\ \mu$s). In addition, this process is particularly sensitive to the atomic temperatures, and provides a new tool for in-situ monitoring of the atomic momentum distribution in an optical lattice. For sufficiently large light-matter couplings, we observe an optical instability for intensities as low as ~ 1 mW/cm^2 in which new, intense beams of light are generated and result in the formation of controllable transverse optical patterns.

OCIS codes: (190.0190) Nonlinear optics; (190.4410) Nonlinear optics, parametric processes; (190.4420) Nonlinear optics, transverse effects in; (020.3320) Laser cooling.

References and links

1. P. Kolchin, R. F. Oulton, and X. Zhang, "Nonlinear quantum optics in a waveguide: Distinct single photons strongly interacting at the single atom level," Phys. Rev. Lett. **106**, 113601 (2011).
2. Q. A. Turchette, C. J. Hood, W. Lange, H. Mabuchi, and H. J. Kimble, "Measurement of conditional phase shifts for quantum logic," Phys. Rev. Lett. **75**, 4710–4713 (1995).
3. R. W. Boyd, *Nonlinear Optics*, 3rd ed. (Academic Press, 2008), Chap. 3.
4. J. Jersblad, H. Ellmann, K. Stochkel, A. Kastberg, L. Sanchez-Palencia, and R. Kaiser, "Non-Gaussian velocity distributions in optical lattices," Phys. Rev. A **69**, 013410 (2004).
5. L. V. Hau, S. E. Harris, Z. Dutton, and C. H. Behroozi, "Light speed reduction to 17 metres per second in an ultracold atomic gas," Nature **397**, 594–598 (1999).
6. H. Michinel, M. J. Paz-Alonso, and V. M. Pérez-García, "Turning light into a liquid via atomic coherence," Phys. Rev. Lett. **96**, 023903 (2006).
7. C. M. Cirloganu, P. D. Olszak, L. A. Padilha, S. Webster, D. J. Hagan, and E. W. V. Stryland, "Three-photon absorption spectra of zinc blende semiconductors: theory and experiment," Opt. Lett. **33**, 2626–2628 (2008).
8. R. W. Boyd, K. Dolgaleva, and H. Shin, "Strong, fifth-order, nonlinear optical response resulting from local-field-induced microscopic cascading in C60," in *Nonlinear Optics: Materials, Fundamentals and Applications* (Optical Society of America, 2009), p. NWB2.
9. D. Felinto, D. Moretti, R. de Oliveira, and J. Tabosa, "Delayed four- and six-wave mixing in a coherently prepared atomic ensemble," Opt. Lett. **35**, 3937–3939 (2010).
10. M. S. Zubairy, A. B. Matsko, and M. O. Scully, "Resonant enhancement of high-order optical nonlinearities based on atomic coherence," Phys. Rev. A **65**, 043804 (2002).
11. C. Hang, Y. Li, L. Ma, and G. Huang, "Three-way entanglement and three-qubit phase gate based on a coherent six-level atomic system," Phys. Rev. A **74**, 012319 (2006).
12. Y. Zhang, U. Khadka, B. Anderson, and M. Xiao, "Temporal and spatial interference between four-wave mixing and six-wave mixing channels," Phys. Rev. Lett. **102**, 013601 (2009).

#153855 - $15.00 USD Received 6 Sep 2011; revised 16 Oct 2011; accepted 20 Oct 2011; published 25 Oct 2011

13. G. Fibich, N. Gavish, and X. P. Wang, "Singular ring solutions of critical and supercritical nonlinear Schrödinger equations," Physica D **231**, 55–86 (2007).
14. A. M. C. Dawes, D. J. Gauthier, S. Schumacher, N. H. Kwong, R. Binder, and A. Smirl, "Transverse optical patterns for ultra-low-light-level-all-optical switching," Laser Photon. Rev. **4**, 221–243 (2010).
15. A. Dawes, L. Illing, S. M. Clark, and D. J. Gauthier, "All-optical switching in rubidium vapor," Phys. Rev. A **308**, 672–674 (2005).
16. M. Saffman and Y. Wang, "Collective focusing and modulational instability of light and cold atoms," in *Dissipative Solitons: From Optics to Biology and Medicine*, Vol. 751 of Lecture Notes in Physics (Springer, 2008).
17. G. A. Muradyan, Y. Wang, W. Williams, and M. Saffman, "Absolute instability and pattern formation in cold atomic vapors," in *Nonlinear Guided Waves and Their Applications* (Optical Society of America, 2005), p. ThB29.
18. Y. Castin and J. Dalibard, "Quantization of atomic motion in optical molasses," Europhys. Lett. **14**, 761–766 (1991).
19. J. Jersblad, H. Ellmann, and A. Kastberg, "Experimental investigation of the limit of Sisyphus cooling," Phys. Rev. A **62**, 051401 (2000).
20. M. Mitsunaga, M. Yamashita, M. Koashi, and N. Imoto, "Temperature diagnostics for cold sodium atoms by transient four-wave mixing," Opt. Lett. **23**, 840–842 (1998).
21. J. A. Greenberg, M. Oriá, A. M. C. Dawes, and D. J. Gauthier, "Absorption-induced trapping in an anisotropic magneto-optical trap," Opt. Express **15**, 17699–17708 (2007).
22. M. Brzozowska, T. M. Brzozowski, J. Zachorowski, and W. Gawlik, "Nondestructive study of nonequilibrium states of cold trapped atoms," Phys. Rev. A **72**, 061401(R) (2005).
23. H.-Y. Lo, Y.-C. Chen, P.-C. Su, H.-C. Chen, J.-X. Chen, Y.-C. Chen, I. A. Yu, and Y.-F. Chen, "Electromagnetically-induced-transparency-based cross-phase-modulation at attojoule levels," Phys. Rev. A **83**, 041804(R) (2011).
24. S. Jonsell, C. M. Dion, A. Kastberg, S. J. H. Petra, and P. Sjolun, "A non-adiabatic semi-classical method for Sisyphus cooling," Eur. Phys. J. D. **39**, 67–74 (2006).
25. A. Yariv and D. M. Pepper, "Amplified reflection, phase conjugation, and oscillation in degenerate four-wave mixing," Opt. Lett. **1**, 16–18 (1977).
26. R. Bonifacio and L. De Salvo, "Collective atomic recoil laser (CARL) optical gain without inversion by collective atomic recoil and self-bunching of two-level atoms," Nucl. Instrum. Methods Phys. **341**, 360–362 (1994).
27. M. G. Moore and P. Meystre, "Theory of superradiant scattering of laser light from Bose-Einstein condensates," Phys. Rev. Lett. **83**, 5202–5205 (1999).

1. Introduction

One area of sustained activity in the field of nonlinear optics is the development of schemes that enable single photons to induce nonlinear optical (NLO) interactions. Single-photon nonlinearities will enhance the efficiency of NLO devices, and are crucial components in quantum information systems. One technique for improving NLO interaction strengths is to increase the electric field strength per photon, such as by placing the NLO material in an optical waveguide [1] or cavity [2]. Alternatively, one can enhance a material's NLO susceptibility by taking advantage of material resonances or carefully designing and preparing the NLO medium [3]. One example of a material that is amenable to both approaches is a gas of atoms, which has the additional advantages that it is generally well-understood (*i.e.*, can be modeled via first principles), can be well-controlled at the quantum level, and has been used to demonstrate extremely large NLO susceptibilities at low light intensities.

Gases of atoms are particularly interesting because both their internal and external degrees-of-freedom can be precisely controlled and act as sources of nonlinearities. Here we report a new dissipation-induced NLO process that leads to the generation of new optical fields when weak, frequency-degenerate optical fields are incident on a cloud of cold atoms. These fields polarize the atoms as well as act on their center-of-mass motion to establish long-range spatial order. The characteristic intensity scale for the NLO process is set by the so-called décrochage intensity I_d discovered in the context of Sisyphus cooling in a photonic lattice. For intensities below I_d, a gas transforms into a non-equilibrium system with two distinct temperature components: a localized cold fraction (f_c, mneumonic c) and a hot fraction (f_h, mneumonic h) undergoing anomalous diffusion [4]. In this regime, the simultaneous spatial localization,

#153855 - $15.00 USD Received 6 Sep 2011; revised 16 Oct 2011; accepted 20 Oct 2011; published 25 Oct 2011

polarization and cooling of the atoms leads to a very efficient NLO response that is dominated by an effective fifth-order ($\chi^{(5)}$) susceptibility. Surprisingly, this fifth-order NLO response is as large as the nonlinearities reported in previous studies that typically involve third-order $\chi^{(3)}$ processes [5]. On an absolute scale, this effective $\chi^{(5)} = 7.6 \times 10^{-15}$ (m/V)^4 is the largest ever reported, exceeding that obtained via electromagnetically-induced transparency (EIT) in a Bose-Einstein condensate by $\sim 10^5$ [6], three-photon absorption in a zinc blend semiconductor by $\sim 10^{22}$ [7], and local-field-induced microscopic cascading in C_{60} by $\sim 10^{25}$ [8].

Materials with an extremely large, controllable fifth-order response have many important applications. They can be used in quantum information networks as new sources of correlated pulse pairs and quantum memories [9] and for performing 3-bit quantum processing [10,11], for example. By controlling the relative contributions of the $\chi^{(3)}$ and $\chi^{(5)}$ NLO response, one can create novel states of light such as liquid light condensates [6] as well as use the interference of the resulting four- and six-wave mixing signals for high-precision measurements and nonlinear spectroscopy [12]. In addition, quintic media can give rise to multidimensional solitons and transverse optical patterns [13], which might be used for low-light-level all-optical switching [14, 15].

At large light-by-light scattering efficiencies, we observe a transition to a collective scattering regime where the back-action of the scattered optical fields significantly affects the center-of-mass motion of the atoms and leads to longer atomic coherence times. Beyond a critical NLO interaction strength, we observe an instability that gives rise to new beams of light. Saffman *et al*. have described theoretically such instabilities in a thermal gas of cold atoms [16, 17] and have shown that the necessary nonlinear interaction strength is smaller than in other media. To the best of our knowledge, this paper represents the first experimental report of mirrorless parametric optical instabilities and pattern formation in cold atoms. Depending on the geometry of the incident beams, the generated light consists of either a sequence of randomly-oriented Gaussian spots or stable multi-petal patterns in the plane transverse to the incident beams' wave vectors.

The organization of this paper is as follows. Section 2 develops the theoretical description of the NLO process, Sec. 3 describes the experimental setup that we use, Secs. 4 and 5 describe the steady-state and transient behavior of the nonlinearity below the instability threshold, respectively, and Sec. 6 discusses the multi-mode fields generated by the optical instability. We summarize our conclusions in Sec. 7.

2. Theory

We consider the geometry shown in Fig. 1a, where optical fields interact with a pencil-shaped cloud of cold atoms with length L and diameter W. We assume that the cloud is highly anisotropic ($L/W \sim 100$), has its long axis aligned along the $\hat{z}$ direction, and has a large on-resonance optical thickness. In order to develop a minimal model that contains the relevant physics, we consider a $J_g = 1/2 \rightarrow J_e = 3/2$ transition, as shown in Fig. 1b. A pair of balanced counterpropagating pump fields (intensity I_p, wave vectors $\pm\vec{k}_p$) with orthogonal linear polarizations (lin$\perp$lin configuration) are incident on the cloud at an angle $\theta = 10^\circ$ relative to the z-axis. Weak signal and idler fields (intensities $I_{s,i}$, wave vectors $\pm\vec{k}_{s,i}$) counterpropagate along $\hat{z}$ and are orthogonally-polarized with respect to the nearly-copropagating pump beams. We refer to the signal and idler fields collectively as probe fields. All fields have frequency ω, which is detuned by $\Delta = \omega - \omega_a$ from the atomic transition frequency ω_a. We note that, while the non-zero value of θ has important implications for phase-matching considerations in the wave-mixing process, it is small enough for us to justify the approximation that the field polarizations all lie in the x-y plane.

#153855 - $15.00 USD Received 6 Sep 2011; revised 16 Oct 2011; accepted 20 Oct 2011; published 25 Oct 2011

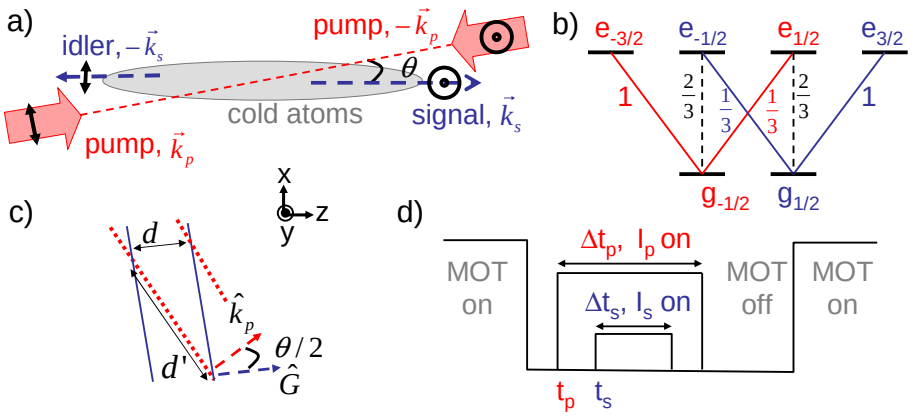

Fig. 1. a) Schematic of the experimental setup. b) Atomic level scheme used in the theoretical model along with the square of the Clebsh-Gordan coefficients (defined as a fraction of the reduced dipole moment μ) for the $J = 1/2 \rightarrow J = 3/2$ transition. c) Optical lattices that form due to the interference of the pump beams (dotted line, $\hat{k}_p$) and a probe and nearly-counterpropagating pump beam (solid line, $\hat{G}$). d) Timing scheme used in the experiment.

We write the total electric field

$$\vec{\mathscr{E}}(\vec{r},t) = \vec{E}(\vec{r},t)e^{-i\omega t} + \text{c.c.}, \tag{1}$$

where $\vec{E} = \sum_n \vec{E}_n \exp(i\vec{k}_n \cdot \vec{r})$ for $n = \{p1, p2, s, i\}$, which corresponds to the two counterpropagating pump, signal, and idler fields, respectively. For our beam geometry, $\vec{k}_{p1} = -\vec{k}_{p2} = \vec{k}_p$ and $\vec{k}_s = -\vec{k}_i$ for $|\vec{k}_n| = k = 2\pi/\lambda$, where $\lambda = 2\pi c/\omega$ and c is the speed of light in vacuum. Motivated by our experimental observations of the polarization configuration that leads to the largest NLO interaction strengths, we choose $\vec{E}_n = \hat{\varepsilon}_n E_n$ for $\{\hat{\varepsilon}_{p1}, \hat{\varepsilon}_{p2}, \hat{\varepsilon}_s, \hat{\varepsilon}_i\} = \{\hat{x}, \hat{y}, \hat{y}, \hat{x}\}$. We take the pump fields $E_{p1} = E_{p2} = E_p$ to be real and constant, the signal and idler fields $E_{s,i} = E_{s,i}(z,t)$ to have slowly-varying, complex amplitudes, and $|E_{s,i}| \ll |E_p|$. We define the beam intensities as $I_n = 2\varepsilon_0 c|E_n|^2$ and assume $I_{s,i,p} \ll I^{\Delta}_{sat}$, where ε_0 is the permittivity of free space, $I^{\Delta}_{sat} = I_{sat}(1 + 4\Delta^2/\Gamma^2)$ is the off-resonance saturation intensity, I_{sat} is the resonant saturation intensity, and Γ is the full width at half maximum natural linewidth of the electronic transition.

These fields produce an atomic polarization

$$\vec{\mathscr{P}}(\vec{r},t) = \overleftrightarrow{\chi}\vec{\mathscr{E}}(\vec{r},t) = \vec{P}(\vec{r},t)e^{-i\omega t} + \text{c.c.}, \tag{2}$$

where $\overleftrightarrow{\chi}$ is the tensor susceptibility. Substituting this polarization into Maxwell's equation yields

$$\left(\frac{\partial \vec{E}_{s,i}}{\partial t} \pm c\frac{\partial \vec{E}_{s,i}}{\partial z}\right) = \frac{i\omega}{2\varepsilon_0}\left\langle \vec{P}e^{\mp i\vec{k}_s\cdot\vec{r}}\right\rangle, \tag{3}$$

where we have made the slowly-varying amplitude approximation and ignored terms proportional to $\exp(\pm 2i\omega t)$. The angular brackets denote a spatial average over a grating period and act to select only the contributions to the polarization that are phase-matched to efficiently drive $E_{s,i}$.

We can consider the full multilevel atomic structure to be equivalent to two V-type transitions where the dynamics of the $g_{\pm 1/2}$ states (mneumonic $\pm$) are identical (up to a spatial offset of $\lambda/4$ discussed later) because the applied fields do not drive π transitions and therefore cannot

#153855 - $15.00 USD Received 6 Sep 2011; revised 16 Oct 2011; accepted 20 Oct 2011; published 25 Oct 2011

establish coherences between the $g_{\pm 1/2}$ states. Thus, we write $\vec{P} = \vec{P}^+ + \vec{P}^-$ and consider the single-atom polarizations $\vec{p}^{\pm}$ such that $\vec{P}^{\pm} = \eta^{\pm}(\vec{r})\vec{p}^{\pm}$, where $\eta^{\pm}(\vec{r})$ is the atomic density at position $\vec{r}$. By adiabatically eliminating the excited state and solving to first-order in the field strengths for $\Delta \gg \Gamma$, we find that

$$\vec{p}^{\pm} = \sum_n \vec{p}_n^{\pm}(\vec{r}) e^{i\vec{k}_n \cdot \vec{r}}, \tag{4}$$

where

$$\vec{p}_n^{\pm}(\vec{r}) = \frac{\overleftrightarrow{\mu}^{\pm}_{eff}}{\hbar\Delta} \cdot \vec{E}_n(\vec{r}) \tag{5}$$

are slowly-varying polarization amplitudes such that $\langle \vec{p}^{\pm} \exp(i\vec{k}_n \cdot \vec{r}) \rangle \sim \vec{p}_n^{\pm} \delta_{nm}$. Here

$$\overleftrightarrow{\mu}^{\pm}_{eff} = \sum_{j=e_{\mp 1/2}, e_{\pm 3/2}} \vec{\mu}_{j,g_{\pm 1/2}} \vec{\mu}_{g_{\pm 1/2},j}, \tag{6}$$

where $\vec{\mu}_{l,j} = \langle j|e\vec{r}|l\rangle$ is the dipole matrix element. Thus, phase-matching requires a spatial modulation of $\eta^{\pm}(\vec{r})$ with wave vectors $\vec{k}_{s,i} - \vec{k}_n$.

We use a perturbative approach to determine the spatially-varying atomic density distribution in the *x*-*z*-plane. We first note that the one-dimensional (1D) photonic lattice along $\hat{k}_p$ formed by the pump beams dominates the atomic motion for $I_{s,i} \ll I_p$. For red detunings ($\Delta < 0$), the atoms load into the anti-nodes of the lattice. This leads to an enhanced atomic polarization because the atoms see a higher average field strength than a homogeneously-distributed sample. In addition, the atoms are optically pumped into the stretched states such that the density modulation due to the pump beam lattice $\eta_p^+(\vec{r}) = \eta_p^+(\vec{r} + q\lambda/2\hat{k}_p) = \eta_p^-(\vec{r} + q\lambda/4\hat{k}_p)$ for integer q, which gives rise to long-range anti-ferromagnetic order. As the atoms move in this bright lattice, Sisyphus (or polarization gradient) cooling changes the atomic momentum distribution from a Maxwell-Boltzmann distribution to one that is well-described by a double-Gaussian [4]. The narrow (broad) Gaussian distribution component corresponds to a cold (hot), bound (unbound) fraction of atoms, which leads to an interpretation of the cooling mechanism as a transfer of population from the hot to the cold fraction. This further allows us to interpret the décrochage intensity as the lattice beam intensity at which nearly all of the atoms have been transferred to the cold fraction, which is equivalent to its original definition as the intensity at which the atomic temperature attains a minimum value (assuming a Maxwell-Boltzmann momentum distribution).

We numerically solve for the momentum distribution $\rho(p)$ along $\hat{k}_p$ in steady-state by using a Bloch-state approach [18] (see Fig. 2a). By fitting the full distribution by a double-Gaussian function, we calculate $f_c = 1 - f_h$ for different values of I_p by considering the fractional area under the narrow Gaussian curve (see Fig. 2b). For the smallest I_p, the momentum distribution is non-normalizable, and f_c is very small and increases slowly with I_p. For larger I_p, $f_c \propto I_p$ before saturating to 1 around $I_p = I_d$, where I_d is independent of Δ [19].

This leads to an anisotropic momentum distribution $\rho(\vec{p})$

$$\rho(\vec{p}) = g(p_y, T_y) g(p_\perp, T_\perp)[f_c g(p_{||}, T_c') + f_h g(p_{||}, T_h')], \tag{7}$$

where $g(p,T) = (2\pi m k_B T)^{-1/2} \exp(-p^2/2mk_BT)$, m is the atomic mass, k_B is Boltzmann's constant, and T_y (p_y), $T'_{c,h}$ ($p_{||}$), and $T_\perp$ ($p_\perp$) correspond to the temperature (momentum) along $\hat{y}$, $\hat{k}_p$, and orthogonal to $\hat{k}_p$, respectively. Typical temperatures in our experiment are $T_y \sim T_\perp \sim T_{eq} = 30\ \mu$K, $T_c' \sim 3\ \mu$K, and $T_h' > 20\ \mu$K.

Despite the fact that the atoms can become well-localized along $\hat{k}_p$, this density grating is not phase-matched for scattering pump light into the probe modes and therefore does not directly

#153855 - $15.00 USD Received 6 Sep 2011; revised 16 Oct 2011; accepted 20 Oct 2011; published 25 Oct 2011

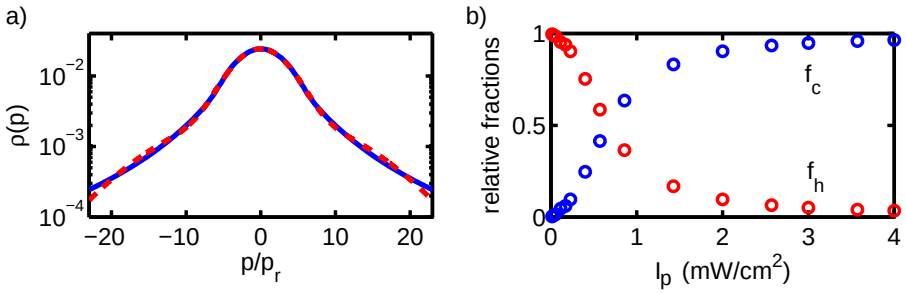

Fig. 2. a) Momentum distribution obtained via numerical simulation (blue, solid line) and a double-Gaussian fit (dashed, red line). $p_r = \hbar k$ is the recoil momentum. b) Fraction of atoms in the hot and cold component as a function of pump intensity.

contribute to the amplification of the signal and idler beams. In contrast, the interference of a probe and nearly-counterpropagating pump field gives rise to a weak additional dipole potential $U^{\pm}$ that perturbs the spatial atomic distribution and produces a density grating along $\vec{G} = \vec{k_p} + \vec{k_s}$ that is phase-matched (see Fig. 1c). Ignoring a constant offset,

$$U^{\pm}(\vec{r}) = U_0^{\pm}\cos(\vec{G}\cdot\vec{r}) = \left(\vec{p}_{p1}^{\pm}\cdot\vec{E}_i^{*} + (\vec{p}_{p2}^{\pm})^{*}\cdot\vec{E}_s\right)e^{i\vec{G}\cdot\vec{r}} + c.c.. \tag{8}$$

For a single-component gas with temperature T along $\hat{G}$, the modulation of the steady-state atomic density distribution produced by $U^{\pm}$ is $\eta_U^{\pm}(\vec{r}) = e^{-U^{\pm}/k_BT}/\langle e^{-U^{\pm}/k_BT}\rangle$. We expand $\eta_U^{\pm}$ in terms of its spatial Fourier modes and find

$$\eta_U^{\pm}(\vec{r}) = 1 - \frac{2I_1(\psi^{\pm})}{I_0(\psi^{\pm})}\cos(\vec{G}\cdot\vec{r}) + ..., \tag{9}$$

where $\psi^{\pm} = U_0^{\pm}/k_BT$ and $I_j(\psi)$ is the modified Bessel function of the first kind. In the regime where $\psi^{\pm} \ll 1$, we Taylor expand Eq. (9) about $\psi^{\pm} = 0$ and find

$$\eta_U^{\pm}(\vec{r}) \sim 1 + b^{\pm}(T)e^{i\vec{G}\cdot\vec{r}} + \left(b^{\pm}(T)\right)^{*}e^{-i\vec{G}\cdot\vec{r}} \tag{10}$$

to first order in $E_{s,i}$, where

$$b^{\pm}(T) = \frac{(\overleftrightarrow{\mu}_{eff}^{\pm}\cdot\vec{E}_{p1})\cdot\vec{E}_i^{*} + (\overleftrightarrow{\mu}_{eff}^{\pm}\cdot\vec{E}_{p2}^{*})\cdot\vec{E}_s}{k_BT\hbar\Delta} \tag{11}$$

corresponds to the degree of atomic bunching in the density grating along $\hat{G}$. Extending this result to the case of our two-component gas, we find that

$$b^{\pm}(T) \rightarrow b^{\pm}(T_c, T_h) = f_c b^{\pm}(T_c) + f_h b^{\pm}(T_h), \tag{12}$$

where $T_{c,h} = T'_{c,h}\cos(\theta/2) + T'_{h,c}\sin(\theta/2) \sim T'_{c,h}$ for $\theta/2 \ll 1$. Thus, the fully-modulated atomic density is

$$\eta^{\pm}(\vec{r}) = \eta\,\eta_p^{\pm}\eta_U^{\pm}/g, \tag{13}$$

where η is the average atomic density and g is the degeneracy of the ground states.

#153855 - $15.00 USD Received 6 Sep 2011; revised 16 Oct 2011; accepted 20 Oct 2011; published 25 Oct 2011

Substituting Eqs. (4) and (13) into Eq. (3) and keeping only phase-matched terms to first order in the probe fields yields

$$\left(\frac{\partial \vec{E}_s}{\partial t}+c\frac{\partial \vec{E}_s}{\partial z}\right) = \frac{i\omega\eta}{2\varepsilon_0}\sum_{j=\pm}\frac{\overleftrightarrow{\mu}^{\pm}_{eff}}{\hbar\Delta}\cdot\left[\vec{E}_s+b^{\pm}(T_c,T_h)\vec{E}_p\right], \tag{14}$$

$$\left(\frac{\partial \vec{E}_i}{\partial t}-c\frac{\partial \vec{E}_i}{\partial z}\right) = \frac{i\omega\eta}{2\varepsilon_0}\sum_{j=\pm}\frac{\overleftrightarrow{\mu}^{\pm}_{eff}}{\hbar\Delta}\cdot\left[\vec{E}_i+\left(b^{\pm}(T_c,T_h)\right)^*\vec{E}_p\right]. \tag{15}$$

Because the time scale associated with the atomic motion is typically much slower than that of the optical fields, we assume that the optical fields follow adiabatically the evolution of the atomic density grating. We therefore take Eq. (14) in steady-state and find

$$\frac{dE_s}{dz} = i\kappa E_s + i\beta E_i^*, \tag{16}$$

$$\frac{dE_i^*}{dz} = i\kappa E_i^* + i\beta E_s \tag{17}$$

where

$$\beta = \beta_c+\beta_h = \frac{2\omega\eta\mu^4 I_p}{9(\varepsilon_0 c\hbar\Delta)^2}\left(\frac{f_c}{k_B T_c}+\frac{f_h}{k_B T_h}\right) \tag{18}$$

$$\kappa = \frac{2\omega\eta\mu^2}{3\varepsilon_0 c\hbar\Delta}+\beta, \tag{19}$$

and μ is the reduced dipole matrix element for the transition.

For an input signal field at z=0 and no input idler field, we find that the normalized output signal and idler intensities are

$$\frac{I_s(L)}{I_s(0)} = \sec^2(\beta L), \tag{20}$$

$$\frac{I_i(0)}{I_s(0)} = \tan^2(\beta L), \tag{21}$$

respectively. The quantity βL therefore corresponds to the nonlinear phase shift imposed upon the probe beams via the NLO interaction. For typical experimental parameters $\eta = 10^{10}$ cm^{-3}, $\mu = 2.53\times10^{-29}$ C·m, $\lambda = 780$ nm, $g = 5$, $\Delta = -5\Gamma$, and $L = 3$ cm for the D2 transition in ^{87}Rb, we find that $\beta L = I_p[100\,f_c(I_p)+13\,f_h(I_p)]$ for I_p in mW/cm^2. Thus, we predict a NLO phase shift of ~ 70 rad for $I_p = 1$ mW/cm^2. We note that the nonlinear dependence of $I_{s,i}$ on η is one type of collective behavior of this NLO system.

The dependence of f_c on I_p (shown in Fig. 2b) gives rise to different NLO regimes. For the smallest pump intensities, $f_c \sim 0$ and $\beta \sim \beta_h \ll 1$. For larger I_p, where $f_c \propto I_p$,

$$\beta_c \propto I_p^2/T_c I_d \tag{22}$$

and

$$\beta_h \propto I_p(1-I_p/I_d)/T_h. \tag{23}$$

Because T_c depends only weakly on I_p and $T_h > 5T_c$ for all I_p, we find that $\beta \sim \beta_c \propto I_p^2/T_c$. We can therefore identify an effective $\chi^{(5)}$ NLO response due to β's locally quadratic dependence on I_p, despite the fact that a true NLO susceptibility does not exist because the Taylor series

#153855 - $15.00 USD Received 6 Sep 2011; revised 16 Oct 2011; accepted 20 Oct 2011; published 25 Oct 2011

expansion about $I_p = 0$ is not valid in this region. This effective $\chi^{(5)}$ response can be understood as six-wave mixing (SWM) involving four optical and two matter wave fields (*i.e.*, the density grating along $\hat{G}$), wherein the pump fields Bragg scatter off the density grating formed via optically-induced atomic cooling and localization. When $I_p > I_d$, the $\chi^{(5)}$ response saturates because $f_c \sim 1$ and we realize an effective $\chi^{(3)}$ response where $\beta \sim \beta_c \propto I_p/T_c$.

While we carried out the previous analysis in steady-state, it is straightforward to extend our results to the transient regime when $\beta L \ll 1$ (*i.e.*, when the back-action of the generated probe fields on the atoms is negligible). If we turn the signal beam off after the system has reached a steady state, the atom's momentum spread gives rise to motion that washes out the density grating and therefore leads to a decay of the pump power scattered into the probe field modes. A 1D Gaussian momentum distribution with a spread $\bar{p} = mu = (2k_BTm)^{1/2}$ leads to a Gaussian decay $\beta(t) \propto \exp(-t^2/\tau^2)$ with $\tau = \Lambda/\pi u$, where Λ is the grating period along the direction of the atomic motion [20]. Extending this result to our multi-component momentum distribution, we expect a multi-Gaussian decay, where the decay times correspond to the effective atomic temperatures. The transient response, therefore, allows us to separately identify the contributions of $\beta_{c,h}$ to the total NLO response.

3. Experimental setup

To create our NLO medium, we use a magneto-optical trap (MOT) tuned to the D2 transition to confine ^{87}Rb atoms in the $F = 2$, $m_f = 2$ state within a cylindrical region with $L = 3$ cm and $W = 300$ μm [21]. The MOT beams consist of two pairs of counterpropagating laser beams: one pair (the radial beams) cools and traps atoms in the *x*-*y*-plane, and the other (the longitudinal beams) cool the atoms along the $\hat{z}$-direction. The radial beams have counter-rotating circular polarizations and an elliptical profile with a semimajor and semiminor axis of 1.5 and 1 cm, respectively. The longitudinal beams have a diameter of 1 cm and arbitrary polarizations (although we typically use a lin$\perp$lin configuration). All MOT beams have a detuning $\Delta = -3\Gamma$ (for $\Gamma/2\pi = 6$ MHz) and intensity I_{MOT}=7 mW/cm^2. Using this setup, we achieve atomic densities of up to $\sim 10^{11}$ atoms/cm^3 for atoms isotropically cooled to $T_{eq} = 30$ μK.

The pump beams used for wave mixing are detuned from the $F = 2 \rightarrow F' = 3$ transition by $|\Delta| = 3 - 25\Gamma$ and have diameters of 3 mm. The incident signal beam is detuned from the pump beams by $\delta = \omega_s - \omega$, has a diameter of 200 μm, and an intensity of $1 - 100$ μW/cm^2 (although $I_s \sim 3$ mW/cm^2 unless otherwise specified). The frequency of the generated idler beam is $\omega_i = \omega - \delta$.

Figure 1c shows the timing sequence for our experiment. First, we cool and trap the atoms for 99 ms with only the MOT beams on. We then turn off the MOT beams and conduct the wave-mixing experiment during the remaining 1 ms, which consists of turning on the pump beams at time t_p for a duration Δt_p. If we want to measure the NLO response below the instability threshold, then we also turn on the incident signal beam at time t_s for duration Δt_s. This cycle is then repeated. We note that, while we leave the MOT magnetic fields on at all times, they do not influence the wave mixing experiment because the atoms are trapped in the region in which the magnetic field is essentially zero. Unlike in a spherical MOT (where magnetic field variations of > 10 G occur for large traps), the longitudinal ($\sim$0 G/cm) and radial (10 G/cm) magnetic field gradients of our anisotropic MOT produce a total magnetic field variation of only 0.3 G across the entire trap. In addition, we have confirmed the negligible role of the MOT magnetic fields by applying additional external fields without adversely affecting the NLO response.

We use independent acousto-optic modulators (AOMs) with response times of < 100 ns to turn the beams on and off as well as scan δ. For experiments where we require $\delta = 0$, we split off a small fraction of the pump beam for use as the signal beam and double-pass it through a separate AOM such that it incurs no net frequency shift. In this way, we can independently

#153855 - $15.00 USD Received 6 Sep 2011; revised 16 Oct 2011; accepted 20 Oct 2011; published 25 Oct 2011

modulate the signal beam amplitude without deleterious effects due to the frequency noise in the AOMs (which is on the order of the spectral linewidth of the NLO resonance).

We record the transmitted signal and generated idler beam intensities via fast photomultiplier tubes (PMTs; Hamamatsu H6780-20) as well as with a fast CCD camera (Dalsa) that images the beams in the far field. We also use separate CCD cameras that directly image the trap fluorescence from the top and side when the MOT beams are present. By calibrating the recorded brightness, we continuously monitor the effective atomic density. In addition, we measure the atomic temperature components along different directions in-situ via recoil-induced resonance (RIR) velocimetry using separate, far-detuned beams [22].

To measure the slow light delay t_d of the atomic sample, we modulate the amplitude of the incident signal beam by 10% at a frequency of 15 kHz and record the intensity of the transmitted beam. We determine the time delay due solely to nonlinear dispersion by comparing the phase of the transmitted signal when $I_p > 0$ to that observed when $I_p = 0$.

4. Steady state response

Figure 3 shows the normalized spectrum of the signal and idler beams in the presence of the pump beams. The features centered around $\delta = \pm 100$ kHz correspond to Raman transitions between vibrational levels of atoms localized in the pump beam lattice. The resonance centered on $\delta = 0$, which is the focus of this paper, arises from Bragg scattering of the pump beams off the density grating along $\hat{G}$ and has a spectral width of $\Delta\omega \sim 30$ kHz. For the remainder of the paper, we consider only the case where $\delta = 0$.

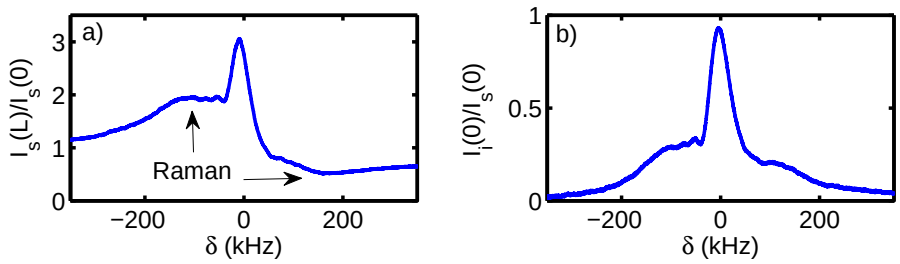

Fig. 3. Normalized intensity spectrum of the a) transmitted signal and b) generated idler beams.

In order to verify the predictions of Eq. (18), we measure the steady-state dependence of $\beta = \beta(I_p, \Delta, \eta, I_s)$. By choosing $t_{p,s} = 0$ and $\Delta t_{p,s}$=1 ms, we monitor $I_{s,i}$ and observe that the system reaches steady-state after ~ 200 μs. We find that the measured steady-state $I_{s,i}$ agree well with Eqs. 20 and 21, which allows us to directly determine βL. Figure 4a shows the measured and predicted (via Eq. (18)) dependence of βL on I_p, where each curve corresponds to a different Δ. In obtaining the fit, we treat the décrochage intensity as a free parameter and find that $I_d \sim 1.5$ mW/cm^2, which is in qualitative agreement with that found in Ref. [19] and is comparable to the resonant electronic-transition saturation intensity $I_{sat} = 1.6$ mW/cm^2.

We first consider the dependence of β on I_p for fixed Δ. For the shallowest lattices, where $f_c \sim 0$, the signal is too small to measure. For slightly larger I_p, where $f_c \propto I_p$, we observe a nearly quadratic dependence of β on pump intensity. Beyond I_d, $f_c \sim 1$ and the SWM process saturates but β continues to increase linearly with I_p. A collective instability occurs for $\beta L > 1$, which gives rise to new beams of light in the absence of incident probe beams (this is discussed further in Sec. 6).

To quantify the strength of the NLO susceptibility, we focus on the case where $\Delta = -3\Gamma$. According to Eqs. 22 and 23, we fit βL with a function of the form $AI_p + BI_p^2$ and find that A

#153855 - $15.00 USD Received 6 Sep 2011; revised 16 Oct 2011; accepted 20 Oct 2011; published 25 Oct 2011

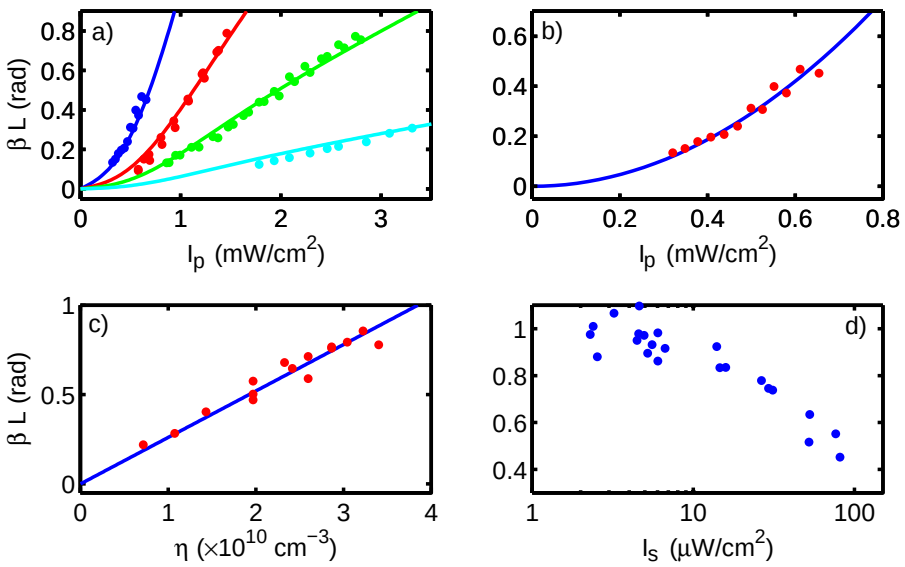

Fig. 4. Dependence of NLO phase shift on experimental parameters. a) Experimental data (points) and theoretical predictions from Eq. (18) (solid curves) for Δ/Γ = -3, -5, -7.3, -12.7 (from left to right, respectively). b) For $I_p < I_d$, the experimental data (points, $\Delta = -3\Gamma$) are well-fit by a quadratic function (solid curve). c) Measured (points) dependence on atomic density and linear fit (solid line) and d) scaling with the incident signal intensity for $\Delta = -5\Gamma$ and $I_p = 1.5$ mW/cm^2.

is negligible and $B = 1.17$ (mW/cm^2)$^{-2}$. This leads to a NLO phase shift of 1.17 rad for $I_p = 1$ mW/cm^2, which is only ~ 60 times smaller than the value predicted via Eq. (18). We attribute this discrepancy to the simplified atomic level structure and perturbative approach used to solve for the atomic motion in the model (*i.e.*, approximating the 2D lattice in terms of two, 1D lattices). B is related to the nonlinear fourth-order index of refraction $n_4 = Bc/2\omega L$ and corresponds to an effective fifth-order susceptibility $\chi^{(5)} \equiv \chi^{(5)}_{xxxxyy} = (c\varepsilon_0)^2 B/45|k_p|L = 7.6\times10^{-15}$ (m/V)^4, which is the largest value ever reported. In addition, we observe nonlinear focusing for $\Delta < 0$, which indicates that the sign of the nonlinearity is such that it increases the gas's nonlinear response (as opposed to other $\chi^{(5)}$ processes that decrease the overall nonlinearity, such as the saturation nonlinearity in two-level atoms).

We next look at the dependence of β on Δ for fixed I_p. In agreement with the predictions of Eq. (18), we find that $\beta \propto \Delta^{-2}$. Because I_d, the effective saturation intensity for the SWM process, is independent of Δ, we can work several Γ away from atomic resonance (where the transmission is high) while simultaneously realizing large NLO interaction strengths. While some degree of absorption is necessary to cool the atoms, the process occurs efficiently (*i.e.*, requires the scattering of few photons) and the deleterious effects due to absorption are minimal. For the data shown in Fig. 4a, we measure a detuning-dependent signal beam transmission of $> 90\%$ in the absence of the pump beams; with the pump beams present, we observe a net amplification of the signal and idler fields.

One metric for quantitatively comparing the NLO response due to this $\chi^{(5)}$ process to previously-measured $\chi^{(3)}$ processes is obtained by considering the achievable nonlinear phase shift for a fixed I_p. For $I_p = 1$ mW/cm^2, we find a phase shift of $\beta L = 1.17$ for $\Delta = -3\Gamma$, which is only 100 times smaller than that reported in Ref. [5] using EIT in a BEC at larger η than

#153855 - $15.00 USD Received 6 Sep 2011; revised 16 Oct 2011; accepted 20 Oct 2011; published 25 Oct 2011

used in our work. Another commonly-used metric in cross-phase-modulation (XPM) experiments is the so-called XPM figure of merit ζ, which is defined as the ratio of the nonlinear phase shift to the power loss [23]. For $\Delta = -3\Gamma$ and $I_p = 1$ mW/cm^2, we measure a power loss of $\ln(0.9) = 0.1$, which leads to $\zeta \sim 12$ and exceeds that typically obtained via EIT [23].

We further verify Eq. (18) by measuring how β depends on η and I_s for a fixed I_p and Δ. Figure 4c shows that β scales linearly with the average atomic density, which indicates that the pump light Bragg scatters coherently off the atomic density grating. In addition, Fig. 4d shows that β is independent of $I_s(0)$ below ~ 15 μW/cm^2. Beyond this the intensity, the nonlinearity begins to saturate and β decreases (see Fig. 4). Thus, Eq. (18) accurately predicts the observed scaling of β over a broad range of all measured parameters.

In addition to a large NLO phase shift, we also observe substantial dispersion at $\delta = 0$. Figure 5 shows the slow-light delay t_d and group velocity $v_g = t_d/L$ as a function of βL for $\Delta = -5\Gamma$. For $\beta L \sim 1$, we observe $v_g/c \sim 10^{-5}$ which acts like a high-finesse cavity and increases the photon lifetime in the gas to several μs, which is comparable to the time scale associated with atomic motion over a distance d. This gives rise to additional effective long-range atom-atom interactions beyond those considered in Sec. 2.

We note that this NLO mechanism is not specific to the particular choice of beam polarizations described up to this point. We observe a similar quadratic scaling of β with I_p for other polarizations that allow for both atomic cooling and bunching (such as linθlin and σ^+-σ^+), although a larger I_p is required to achieve the same NLO phase shifts. For dark lattices, where $\Delta > 0$, we still observe an amplification of the signal beam, but $\beta \sim 100\times$ smaller than in the case of the bright lattice for a given I_p. We attribute this red-blue asymmetry to the fact that, while the atoms still become spatially organized for $\Delta > 0$, they load into the intensity nodes (thereby minimizing their polarization) and undergo heating at low beam intensities. Thus, these results further validate our physical interpretation of the NLO process as being dependent on both atomic bunching and cooling in the photonic lattice.

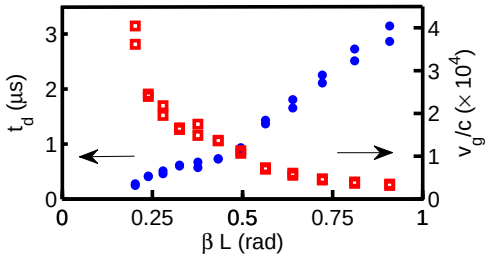

Fig. 5. Dependence of the slow-light delay and group velocity on the NLO coupling strength for $\Delta = -5\Gamma$.

5. Transient response

In this section, we investigate the NLO process in the transient domain. Figure 6 shows the growth of β in time, where we turn the signal beam on at $t = 0$. We turn the pump beams on at $t = 0$ for the lower (red) curve and find that the process of cooling and loading of atoms into the grating along $\hat{G}$ occurs over ~ 200 μs. We observe that the grating formation time is reduced to ~ 25 μs (upper blue curve) when we separately turn the pump beams on at $t = -400$ μs and then turn the signal beam on at $t = 0$. The density grating along $\hat{G}$ forms more quickly in this case because the atoms have already been cooled and localized along $\hat{k}_p$ by the pump beam lattice during the 400 μs prior to $t = 0$. This ~ 25 μs time scale is consistent with the time it

#153855 - $15.00 USD Received 6 Sep 2011; revised 16 Oct 2011; accepted 20 Oct 2011; published 25 Oct 2011

takes atoms confined in the pump beam lattice with $T_\perp = T_{eq}$ to load into the grating along $\hat{G}$ by moving a distance $d' = \lambda/2\sin(\theta/2)$ in the direction orthogonal to $\hat{k}_p$ (see Fig. 1c) under the influence of $U^{\pm}$.

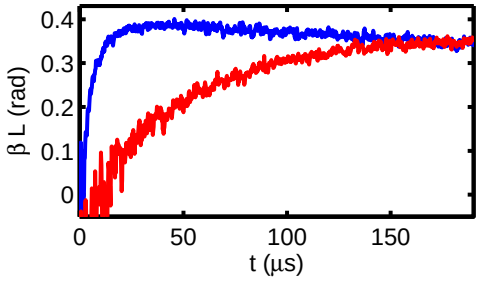

Fig. 6. (Color online) Growth of βL as a function of time when the signal beam turns on at $t = 0$. The lower red (upper blue) curve corresponds to the case where we turn the pump beams on at $t = 0$ ($t = -400$ μs) for $\Delta = -5\Gamma$.

We can measure $\beta_{c,h}$ directly by studying the SWM signal decay after we turn off the incident signal beam (while the pump beams remain on). As discussed in Sec. 2, a finite atomic momentum spread leads to motion that washes out the density grating. Thus, we can separate out the contributions to $\beta_{c,h}$ according to the observed decay time because each has a distinct temperature associated with it. In addition, when t_d and $I_{s,i}$ are small enough for us to ignore the back-action of the fields on the atomic motion (*i.e.*, $\beta L \ll 1$), we can directly extract the effective temperatures.

Figure 7 shows $\beta(t)$ after the incident signal field is extinguished at $t = 0$. For small I_p, where almost all of the atoms are in the hot, unbound component, $\beta_c \sim 0$ and β_h decays after a time $\tau_h = 1.8$ μs (see Fig. 7a), which corresponds to $T_h = 25$ μK for $\Lambda = d$. Increasing I_p increases f_c and gives rise to a second Gaussian decay component due to the cold atomic fraction. We independently measure $T_c \sim 3$ μK, which implies that the atoms are bound in the pump beam lattice and grating decay along $\hat{G}$ is highly suppressed. Therefore, atomic motion in the direction perpendicular to $\hat{k}_p$ determines the decay time for β_c. By fitting the decay in Fig. 7b with a double-Gaussian, we find that $\tau_c \sim 20$ μs, which corresponds to $T_\perp = T_{eq}$ for $\Lambda = d' = 11.5d$.

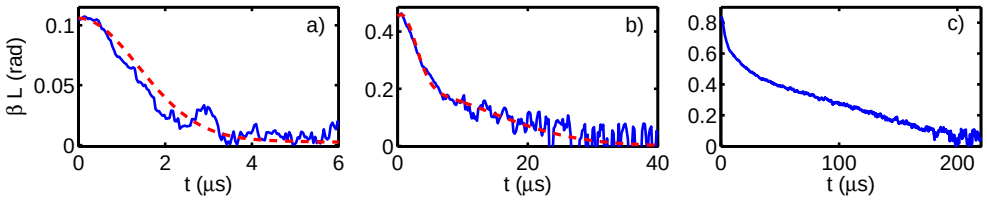

Fig. 7. Decay of the nonlinear coupling coefficient as a function of time after the signal beam is turned off at $t = 0$ for $\Delta = -5\Gamma$ and I_p = a) 0.45, b) 0.7 and c) 1.25 mW/cm^2. The solid and dashed lines correspond to experimental data and a double-Gaussian fit, respectively (note the change in scale of the horizontal axis).

For larger I_p where $\beta L > 0.5$, the back-action of the amplified probe fields strongly influences the coupled light-matter dynamics. In this regime, additional cooling along the direction perpendicular to $\hat{G}$ begins to occur via the lattice formed by the pump and nearly-copropagating

#153855 - $15.00 USD Received 6 Sep 2011; revised 16 Oct 2011; accepted 20 Oct 2011; published 25 Oct 2011

probe beams and reduces $T_\perp$. Atoms cooled in both the x- and z-directions give rise to a third decay time, as shown in Fig. 7c. In addition, the large values of t_d invalidate our assumption that the field evolution is slaved to the atomic motion and prevents us from directly extracting a temperature from the observed decay time. Nevertheless, the strong coupling between the evolution of the atomic and optical fields represents a secondary form of collective behavior and leads to the observation of long coherences times of $> 100\ \mu$s.

We use a multi-Gaussian function to fit $\beta(t)$ for various I_p and relate the amplitudes associated with the slow and fast decay components with $\beta_{c,h}$, respectively. Figure 8 shows the dependence of $\beta_{c,h}$ on I_p for $\Delta = -5\Gamma$. We find that the predictions of Eqs. 22 and 23 agree reasonably well with the experimental results, where we use $f_{c,h}(I_p)$ shown in Fig. 2 and $T_c/T_h = 10$. The main source of discrepancy between the measured and predicted values stems from the oversimplified model used to determine $f_{c,h}$ [24]. Instead, we can consider this approach to represent a new technique for independently determining $f_{c,h}$, as our method is particularly sensitive to the small cold fraction and works in the region $I_p \ll I_d$. Thus, this technique may be useful for building a phenomenological model of Sisyphus cooling well below décrochage.

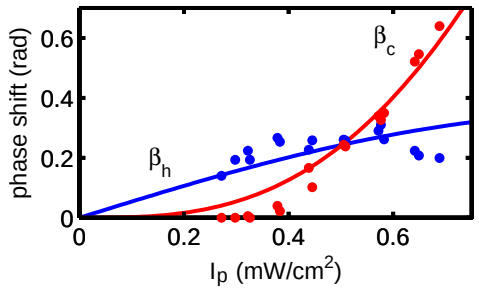

Fig. 8. Dependence of $\beta_{c,h}$ on I_p. Points correspond to experimental data extracted from multi-Gaussian fits to the transient decay measurements, and the solid curves are obtained by a fit using Eqs. 22 and 23.

6. Transverse optical instabilities

We observe an optical instability that generates new beams of light for $\beta L > 1$, which occurs for pump intensities as low as 1 mW/cm^2 and can be understood as either parametric self-oscillation [25] or collective scattering [26]. We consider first the geometry shown in Fig. 1a, where we shine only the pump beams on the atoms. We find that light is emitted in the signal and idler modes (*i.e.*, the direction of maximum gain), which implies that initial density fluctuations are amplified via the NLO process and lead to a spontaneous, long-range spatial organization along $\hat{G}$. The profile of the generated light in the x-y plane is roughly Gaussian and aligned with the center of the trap, but we find that multiple modes (within a few mrad angular width) can fire sequentially within a single shot (*i.e.*, MOT realization). This result is similar to the predictions of Moore *et al.* [27], where multi-mode emission occurs via an atomic-bunching-induced instability in an anisotropic BEC. In addition, we note that the instability only occurs for $\Delta < 0$, in agreement with the physical mechanism described above but contrary to previously-observed wave mixing instabilities based on electronic nonlinearities (which typically require $\Delta > 0$).

Figure 9 shows the measured time-dependent intensity of the generated light in the signal and idler modes (where we turn the pump beams on at $t = 0$). While the details of $I_{s,i}(t)$ vary from shot-to-shot, we observe several universal characteristics. Immediately after turning the pump beams on, there is a period of time (typically lasting 20-50 μs and dependent on I_p)

#153855 - $15.00 USD Received 6 Sep 2011; revised 16 Oct 2011; accepted 20 Oct 2011; published 25 Oct 2011

during which the atoms are cooled and the density grating forms. After this time, we observe an exponential growth of the intensity before it reaches a maximum value of $\sim 0.1 I_p$. The generated light persists and displays complicated temporal dyanmics for several hundred μs, after which time free expansion of the MOT in the y-direction reduces η and $I_{s,i}$ decreases. We note that the signal and idler modes show strong temporal correlations of $r > 0.9$ (where r=(-)1 for perfectly (anti-)correlated signals) due to their mutual coupling.

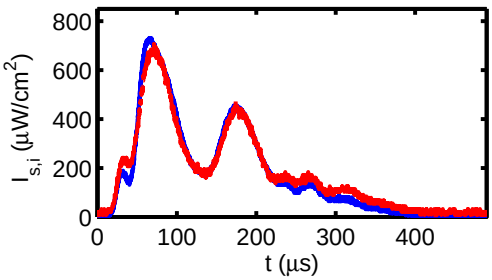

Fig. 9. Time-dependent intensity of the instability-generated light in the $+\hat{z}$ (signal, red) and $-\hat{z}$ (idler, blue) directions for $I_p = 5$ mW/cm^2 and $\Delta = -5\Gamma$, where the instability threshold is $I_p = 2.3$ mW/cm^2. The temporal correlation of the signal and idler modes is $r = 0.99$.

If we alter the beam geometry such that the pump beams propagate along $\hat{z}$ and are focused down to a diameter on the order of W (see Fig. 10a), we observe multi-petal transverse optical patterns generated in both the $\pm\hat{z}$ directions. Because the focused pump beams weakly confine the atoms in the x-y plane, the patterns can persist for ~ 2 ms (where we modify our experimental timing scheme to allow for a 2-ms-long wave-mixing period). Depending on the relative powers and exact alignment of the pump beams, we find many different types of patterns. Figure 10b shows several examples of patterns, including two-, four-, and six-spot patterns as well as a nearly-continuous ring. In addition, we can choose a configuration where the orientation of the patterns rotate randomly (when there is a high degree of symmetry) or are fixed in a particular orientation (when we impose an asymmetry externally).

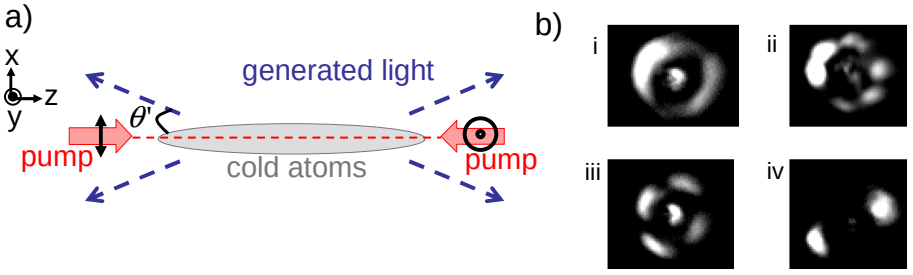

Fig. 10. a) Beam geometry for pattern-forming instability, where $\theta' \sim 5$ mrad. b) Transverse optical patterns, including i) a nearly full ring and ii) a six- iii) four- and iv) two-spot pattern, for $I_p = 15$ mW/cm^2, $\Delta = -8\Gamma$ and an instability threshold of $I_p = 6$ mW/cm^2. The central spot in the images corresponds to residual pump light.

For the highly-symmetric case, we find that we can inject a weak control beam along the cone of the generated light and pin the pattern orientation. In the case where a particular pattern orientation is set by a broken symmetry in the system, we find that we can use the control beam

#153855 - $15.00 USD Received 6 Sep 2011; revised 16 Oct 2011; accepted 20 Oct 2011; published 25 Oct 2011

to rotate the pattern to a specified orientation. Thus, we anticipate that this system may be useful for low-light-level all-optical switching applications [14, 15].

7. Conclusions

In this paper, we present the theory for and experimental demonstration of a new, dissipation-induced NLO process that arises when a cloud of cold atoms are simultaneously polarized, spatially-organized, and cooled by incident optical fields. By using a weak beam to probe the atomic NLO response, we observe that a regime exists for which the NLO coupling strength scales quadratically with I_p and SWM occurs. This corresponds to an extremely large fifth-order nonlinearity, and leads to substantial NLO phase shifts with high transparency.

For sufficiently large NLO coupling strengths, we enter a regime in which the back-action of the amplified probe fields strongly influences the system dynamics. This leads to additional atomic cooling, enhanced atomic coherence times, slow optical group velocities, and, eventually, optical instabilities and pattern formation.

#153855 - $15.00 USD Received 6 Sep 2011; revised 16 Oct 2011; accepted 20 Oct 2011; published 25 Oct 2011